JVSTB Journal of Vacuum Science & Technology B

Single-crystalline silver film grown on Si (100) substrate by using electron-gun evaporation and thermal treatment

Bo-Tsun Chou, Sheng-Di Lin, Bo-Hao Huang, and Tien-Chang Lu

Citation: Journal of Vacuum Science & Technology B **32**, 031209 (2014); doi: 10.1116/1.4874618
View online: http://dx.doi.org/10.1116/1.4874618
View Table of Contents: http://scitation.aip.org/content/avs/journal/jvstb/32/3?ver=pdfcov
Published by the AVS: Science & Technology of Materials, Interfaces, and Processing

Single-crystalline silver film grown on Si (100) substrate by using electron-gun evaporation and thermal treatment

Bo-Tsun Chou and Sheng-Di Lin[a)]
Department of Electronics Engineering, National Chiao Tung University, 1001 University Road, Hsinchu 30010, Taiwan

Bo-Hao Huang and Tien-Chang Lu
Department of Photonics Engineering, National Chiao Tung University, 1001 University Road, Hsinchu 30010, Taiwan

(Received 20 January 2014; accepted 22 April 2014; published 2 May 2014)

The authors demonstrate a simple method to fabricate ultrasmooth single-crystalline silver (Ag) films with high reflectivity and low plasmonic damping. The single-crystalline Ag thin film on the clean Si (100) substrate is first deposited by electron-gun evaporator and then treated by rapid thermal annealing (RTA) to improve its quality. The crystal structure and surface morphology are characterized by x-ray diffraction, transmission electron microscopy, and atomic force microscopy. Optical constants of the prepared films are extracted by fitting the measured reflectivity spectra with the Drude model. These results show that the Ag film with 340 °C RTA has the best film quality, including small surface roughness of 0.46 nm, a sharp x-ray diffraction peak with FWHM of 0.3°, and lowest damping in the visible and near-infrared wavelength regime. Therefore, our method is not only cost-effective but also useful for fabricating metal-based plasmonic and nanophotonic devices. © *2014 American Vacuum Society*. [http://dx.doi.org/10.1116/1.4874618]

I. INTRODUCTION

Nanoscale lasers have been a blooming research topic in recent years, including plasmonic lasers[1–4] and metallic nanocavity lasers.[5–8] In these works, silver is the most-often used noble metal due to its lowest optical loss and minimal plasmonic damping at the visible and near-infrared regime.[9] It is worth noting that high-quality single-crystalline metal films play a key role in boosting the performance of various plasmonic devices.[4] However, to fabricate single-crystalline Ag films is a daunting challenge because the Ag atom arrangement could be sensitive to the template surface construction and cleanness. In past decades, there were a few works reporting preparation of single-crystalline metal films using ultrahigh vacuum (UHV) chamber with an extremely low growth rate[10–13] as the UHV chamber provides an ultra clean environment to prevent the surface from oxidation before the growth. Hanawa and Oura[11] grew single-crystalline Ag (100) film on silicon (100) wafer at room temperature in an UHV chamber ($1 \sim 2 \times 10^{-10}$ Torr). Their growth procedure started with flashing the silicon wafer to ~1200 °C several times to desorb the native oxide and then deposited Ag at a rate of 0.5 nm/min. Hoegen *et al.*[12] also prepared Ag (111) thin films on the Si (100) substrate in a UHV chamber by using a two-step method. The Ag film was deposited at low temperature (90 ~ 130 K) and then annealed to room temperature. Then, the single-crystalline Ag film was formed during the annealing procedure as Ag atoms were rearranged into a periodic array. Similar method was performed by Smith *et al.*[13] to fabricate the atomic-flat Ag film on the GaAs (110) substrate although the sample size is in micrometer to millimeter scale. Recently, Chen *et al.*[14] demonstrated a simple and cost-effective method to grow a smooth and low-loss Ag film. They deposited germanium (Ge) wetting layer first before the electron-gun (e-gun) deposition of Ag. The Ge layer greatly reduced the film roughness so a large-scale, uniform and continuous Ag film was obtained. However, the resultant Ag film was polycrystalline.

Different from the previous time- and cost-consuming methods,[10–14] we have developed an easy and cost-effective way to fabricate a thickness controllable, large-area, high-quality and single-crystalline Ag film, which could benefit the development of Ag-based plasmonics. Our method employs *ex-situ* e-gun evaporation followed by rapid thermal annealing (RTA) by using the conventional semiconductor process equipment. The transmission electron microscopy (TEM) analysis and x-ray diffraction (XRD) data reveal that the grown Ag film is indeed single-crystalline. The surface morphology images taken by atomic force microscopy (AFM) and the optical reflectivity spectra are investigated. By fitting the reflectivity spectra with Drude theory, the damping factor, which is a crucial parameter for plasmonic devices, is extracted for our Ag films. By optimizing the rapid thermal annealing treatment temperature, we can obtain a single-crystalline Ag film with smooth surface and excellent optical properties.

II. EXPERIMENTAL AND MEASUREMENT SETUP

The following surface cleaning procedure is crucial for preparing the high-quality Ag films on the substrate. The undoped Si (100) wafers were rinsed in deionized (DI) water for 5 min and then processed with the four-step cleaning. First, the wafers were immersed into a hot (85 °C) solution of H_2SO_4:H_2O_2 (3:1) for 15 min, rinsed in DI water for 5 min, and then dipped in HF:H_2O (1:100) solution for

[a)]Electronic mail: sdlin@mail.nctu.edu.tw

$10 \sim 15$ s. Second, a 15-min immersion in a hot (85 °C) solution $NH_4OH:H_2O_2:H_2O$ (1:4:20) was introduced and followed by DI water rinse for 5 min. Subsequently, the wafers were put into a 85 °C solution of $HCl:H_2O_2:H_2O$ (1:1:6) for 15 min and, again, rinsed in DI water for 5 min. Finally, we dipped the silicon wafer in $HF:H_2O$ (1:100) solution several times until the wafer surface was hydrophobic, indicating that the Si surface was hydrogen-terminated. To avoid surface oxidation, the silicon wafers were loaded into the e-gun evaporation chamber immediately. We used an e-gun evaporation system (ULVAC EBX-8C) to deposit Ag films of 200-nm thickness. The purity of the Ag source was 99.99% provided by Gredmann Corporation. Before the evaporation, the chamber pressure was about 1×10^{-6} Torr and the growth rate was about 0.02 nm/s for the first 5 nm and about 0.3–0.5 nm/s for the rest. The evaporation rate and the film thickness were monitored in real time with a quartz crystal oscillator. Afterward, RTA treatments were performed to optimize the quality of the grown films. The samples were, respectively, heated up in 20 s to six annealing temperatures from 320 to 420 °C in a step of 20 °C for 60 s in flowing nitrogen.

We observed the surface morphologies and root-mean-square (RMS) roughness of the specimens with and without RTA treatments by AFM (Veeco D3100) in a noncontact tapping mode at room temperature. The typical scanning size was $1 \times 1\ \mu m^2$ and the scanning rate was 1 Hz. We also measured the normal incident reflectivity spectra from 200 to 1000 nm (N&K 1500) with a spot size of about 1 mm. To analyze their crystal structures, the Ag films were characterized by XRD and TEM. The ω-2θ scanning high-resolution XRD ($\lambda = 0.154$ nm, Bede D1) was used to analyze the Ag films by scanning the 2θ from 30° to 85°. In addition, Ag films were polished mechanically and then by ion milling to prepare specimens for TEM analysis. During polishing procedure, we kept the sample temperature below 150 °C to prevent the Ag thin films from the reannealing effect. The thickness of the thinnest region of the specimen was about 50–80 nm. The TEM specimens were stored in a vacuum box immediately after preparation to avoid oxidation. The analysis was performed in a TEM system with a field emission gun (JEOL, JEM-2100F) at room temperature.

III. RESULTS AND DISCUSSION

A. Crystal structure and surface morphology

The XRD analysis of the Ag thin films is shown in the inset of Fig. 1(a); there are only two peaks observed with 2θ scan in all the specimens: one is at ~44° and the other at ~69°. The peak at 69° corresponds to Si (400) which is contributed from the Si substrate and the peak at 44° arises from Ag (200). The XRD results indicate that the Ag thin films are indeed single crystalline as they have the only one diffraction peak at 44°. Although the peak intensities of Si (400) are almost the same in all samples, those of Ag (200) are quite different as we can see in the enlarged XRD spectra in Fig. 1(a). To make it clear, we have plotted the XRD peak intensity and the corresponding full-width at half-maximum

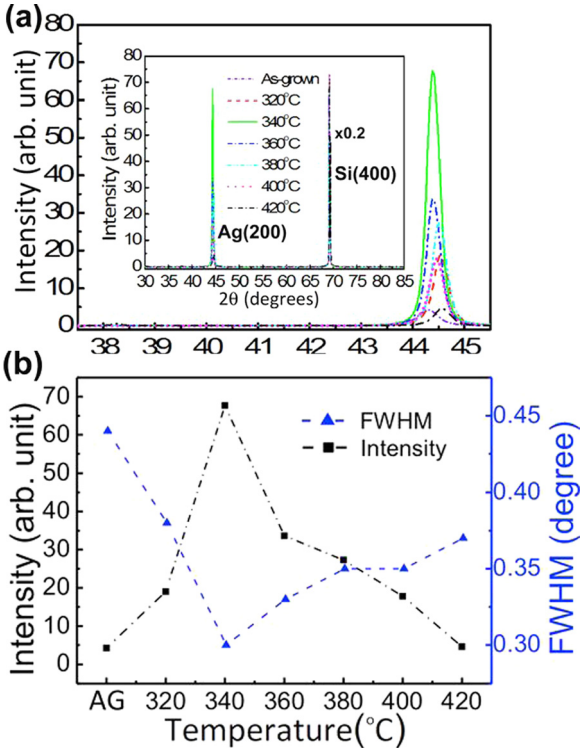

FIG. 1. (Color online) (a) XRD analysis of the Ag films with and without RTA treatments. The inset of (a) shows the XRD 2θ scan results from 30° to 85° of all the Ag specimens. (b) XRD peak intensity and FWHM as a function of the annealing temperature.

(FWHM) of all samples in Fig. 1(b). The peak intensity (square symbols) of the as-grown (AG) Ag film is very weak (~5) but increases 14-fold to ~70 after RTA at 340 °C. For the films with higher annealing temperature, the intensity decreases considerably. On the other hand, as seen in Fig. 1(b), the FWHM of the as-grown Ag (200) peaks Ag film is about 0.44°. The smallest FWHM of 0.3° occurs again with the sample with 340 °C RTA. In short, the XRD results indicate that the RTA can improve the Ag crystal structure, and the optimized temperature is 340 °C.

Figure 2 shows the bright-field TEM picture taken from the Ag film with RTA at 340 °C. The upper layer is the Ag film and bottom one is the Si (100) substrate. We can see a clear interface between Ag and Si with a 2-nm-thick intermixing layer. The nearly perfect, atomiclike periodic array in the Ag film (which is also seen in the Si substrate) reveals that the Ag film is of high-quality and indeed single crystalline. This is further confirmed with the diffraction pattern analysis on the same sample, which is shown in the inset of Fig. 2. The clear and sharp hexagonal diffraction pattern without any observable side points is consistent with the faced cubic center (FCC) structure of Ag. The long axis of the hexagonal is Ag (100) direction. In addition, we obtained the almost same images at two different locations distant from each other for about 5 μm, indicating the good uniformity of the film.

The AFM images of our Ag films are illustrated in Fig. 3. In Fig. 3(a), the surface morphology of the as-grown Ag film is relatively rough and islandlike with a RMS roughness of

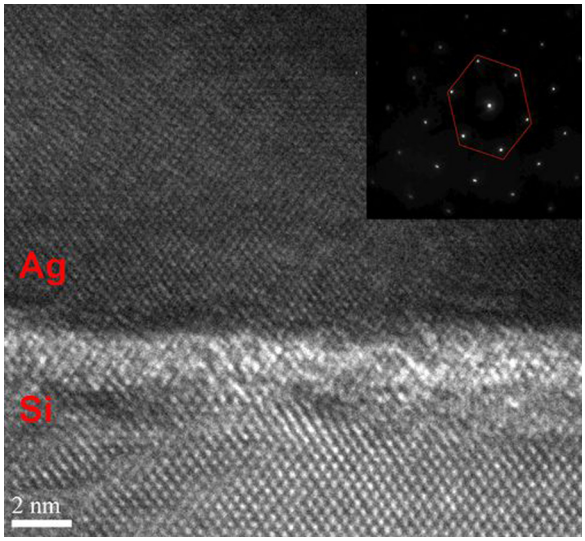

FIG. 2. (Color online) Bright-field TEM picture taken from the Ag film with RTA at 340 °C. The inset is the electron diffraction pattern. The pattern is a hexagon and the long axis direction is Ag (100).

3.39 nm. With the post RTA at 340 °C, a much smoother surface profile [see Fig. 3(b)] is obtained with a RMS roughness of 0.46 nm. This value is superior to previous results.[14,15] However, for the sample with RTA temperature of 420 °C, the surface roughness increases again as shown in Fig. 3(c). We summarize the AFM results in Fig. 4 for two scanning areas of 1×1 and $5 \times 5\ \mu m^2$. The roughness of AG Ag thin film is between 3.0 and 3.5 nm. That decreases dramatically to about 0.5–1.0 nm as the post RTA is performed probably due to that the Ag islands reflow and form a smooth surface. A good temperature range for RTA is 320–380 °C, but the best one is 340 °C. For the RTA temperatures higher than 380 °C, it seems that Ag atoms pile up and result a moonlike surface. The surface roughness of a metal film is important to plasmonic and photonic devices such as superlenses, hyperlenses,[16–20] and surface-plasmonic-polariton (SPP) devices.[21–23] It is worthy to note that the Ag film with 340 °C RTA has the surface roughness comparable to that grown by the molecular beam epitaxy method.[13]

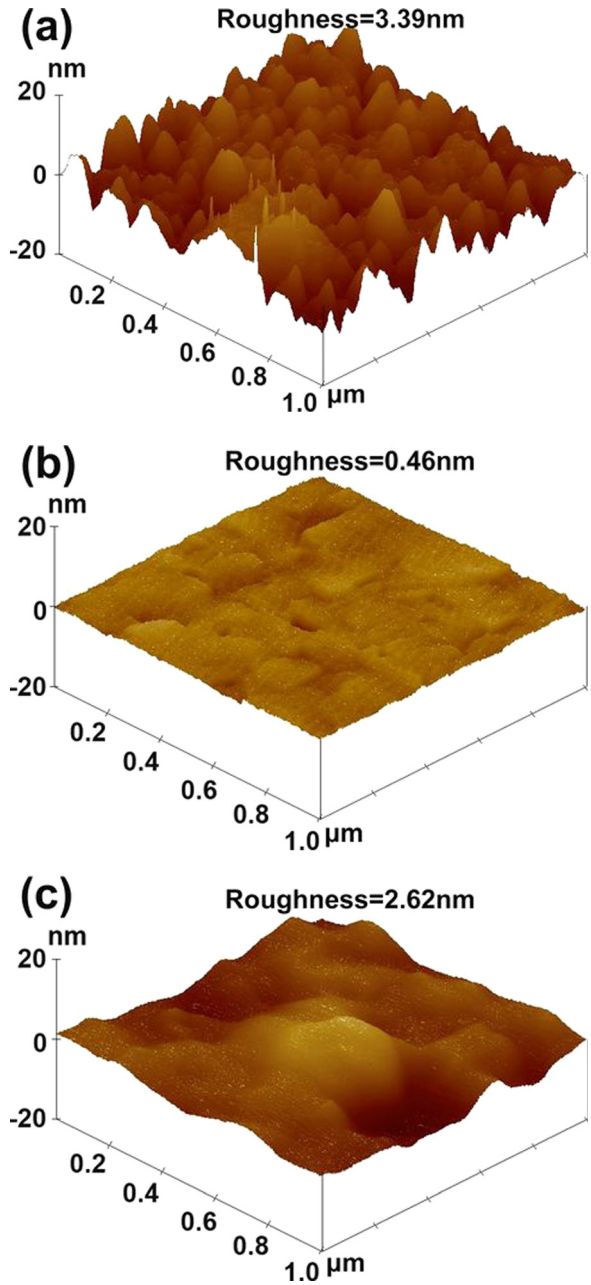

FIG. 3. (Color online) $1 \times 1\ \mu m^2$ bird-view AFM images of the Al films: (a) as-grown, (b) RTA at 340 °C, and (c) RTA at 420 °C.

B. Optical properties

The measured reflectivity spectra of the Ag thin films are plotted in Fig. 5. As we can see in the inset of Fig. 5, the reflectivity approaches ~ 1.0 at the wavelength longer than 500 nm. The reflectivity discrepancy among samples can be spotted in the wavelength range from 320 to 420 nm as shown in Fig. 5. The reflectivity dip around 320 nm (~4 eV) arises from the absorption of interband transition in Ag.[24] In the range of 340–360 nm, the Ag films with RTA at 320–380 °C exhibit slightly higher reflectivity comparing with others.

To quantitatively explain the reflectivity discrepancy, we extracted the optical parameters of those Ag films by fitting the measured reflectivity spectra with the Drude model.[24,25] In the following, we shall first discuss the dependence of the scattering time on annealing temperature and then we use the obtained scattering time (τ) of each sample to calculate the complex relative dielectric constant ($\varepsilon_{r,R} + i\varepsilon_{r,I}$). In the Drude model, the real and imaginary parts of the complex permittivity for metals can be expressed as below, respectively,[24,25]

$$\varepsilon_{r,R} = \frac{\varepsilon_\infty}{\varepsilon_0} - \frac{\omega_p^2 \tau^2}{1 + \omega^2 \tau^2}, \tag{1}$$

$$\varepsilon_{r,I} = \frac{\omega_p^2 \tau}{\omega(1 + \omega^2 \tau^2)}, \tag{2}$$

where ω_p is the plasmon frequency of Ag. ω is the angular frequency of the incident light. For silver, $\varepsilon_\infty = 4.785\varepsilon_0$

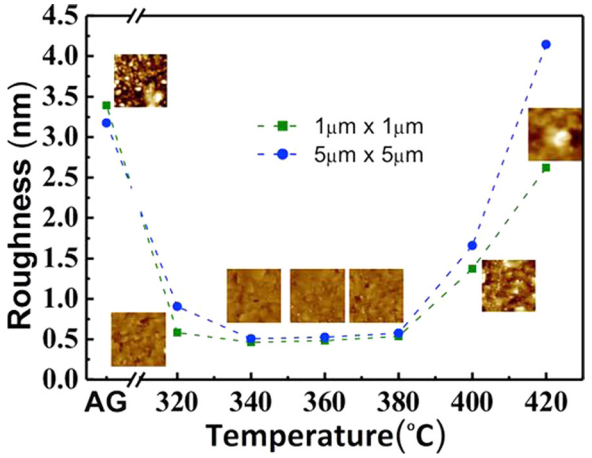

FIG. 4. (Color online) Roughness and morphologies for all samples. The circular and square symbols represent, respectively, the RMS taken from the areas of 5×5 and $1 \times 1\ \mu m^2$.

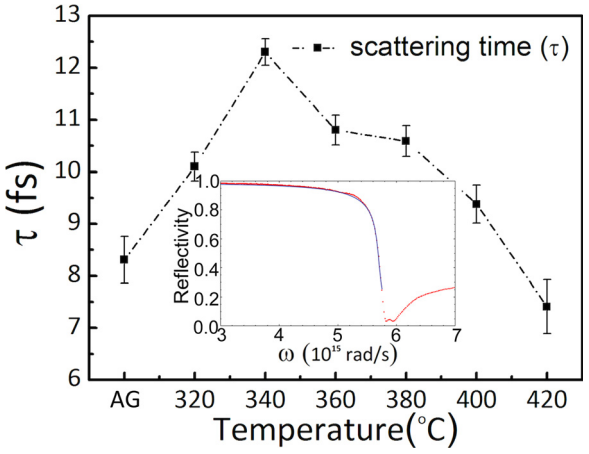

FIG. 6. (Color online) Scattering time as a function of the annealing temperature. Inset: measured and fitting reflectivity of the Ag film with RTA at 340 °C.

which considers the polarization of the background.[24,25] τ is the scattering time, the other fitting parameter used here. The refractive index n and κ can be obtained accordingly

$$n^2 = \frac{1}{2}\left[\varepsilon_{r,R}(\omega) + \sqrt{\varepsilon_{r,R}^2(\omega) + \varepsilon_{r,I}^2(\omega)}\right], \tag{3}$$

$$\kappa^2 = \frac{1}{2}\left[-\varepsilon_{r,R}(\omega) + \sqrt{\varepsilon_{r,R}^2(\omega) + \varepsilon_{r,I}^2(\omega)}\right]. \tag{4}$$

And the reflectivity (R) can be calculated from Eqs. (3) and (4) as

$$R = \frac{(n-1)^2 + \kappa^2}{(n+1)^2 + \kappa^2}. \tag{5}$$

By using Eq. (5), we do the spectra fitting in the range of 2×10^{15} to 5.8×10^{15} rad/s with only two fitting parameters, ω_p and τ, in the following way. The sudden drop of reflectivity around 330 nm is a common feature among samples. We found that $\omega_p = 1.25 \times 10^{16}$ rad/s (corresponds to $\lambda_p = 150.7$ nm) is needed to obtain the well-fitting of this drop so we fixed this parameter for all samples. The other fitting parameter τ is then used to fit the respective reflectivity spectra. As an example, the inset of Fig. 6 shows the well-fitting result of the Ag film with RTA at 340 °C. The dot and solid lines represent the measured and fitting data, respectively. The extracted scattering times τ of Ag films are plotted in Fig. 6. For the AG Ag film, τ is 8.3 fs. The scattering time increases to 12.3 fs for the film with 340 °C RTA, indicating that the mean free path between collisions becomes longer. For the films with higher annealing temperatures, however, the scattering times decrease. Eventually, the scattering time of the film with 420 °C RTA is shorter than that of the as-grown film. Based on this result, we can expect that the Ag film with 340 °C RTA could have the lowest plasmon damping. This trend is also consistent with the surface roughness data in Fig. 4. We have to note that, because the interband absorption and other loss mechanisms have been ignored in our model, the scattering times obtained here is only for comparison between the Ag films with different RTA conditions.

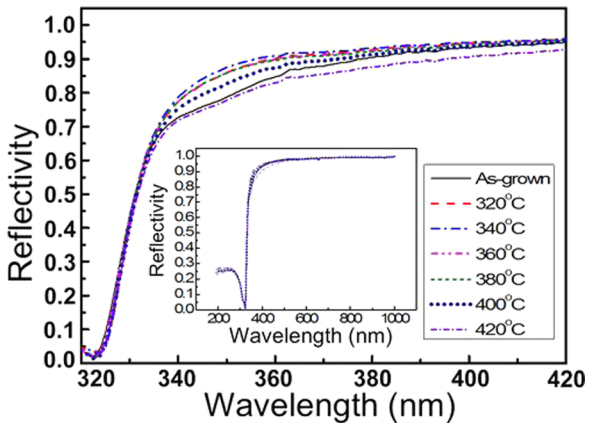

FIG. 5. (Color online) Reflectivity spectra of all the Ag films. Inset: the reflectance spectra from 200 to 1000 nm.

Finally, we have used Eqs. (1) and (2) with the extracted scattering times τ to calculate the complex relative dielectric constant in the range of 400–1000 nm, as illustrated in Fig. 7. As shown in Fig. 7(a), the real part of complex relative dielectric constant $\varepsilon_{r,R}$ decreases from about -2.25 to -39.17 when the wavelength increases from 400 to 1000 nm. No significant difference between the Ag films is spotted. On the other hand, the imaginary part of complex relative dielectric constant $\varepsilon_{r,I}$ deserves more attention because it relates to its electromagnetic loss.[25,26] The imaginary part of complex relative dielectric constant ($\varepsilon_{r,I}$) of all Ag films is shown in Fig. 7(b). $\varepsilon_{r,I}$ increases with the increasing wavelength because the nonzero extinction coefficient (κ) causes an exponential decay for the electromagnetic wave propagating in a lossy medium. For almost all wavelengths, $\varepsilon_{r,I}$ of the as-grown Ag film is the second largest. It lowers as the RTA treatment is taken place. The lowest $\varepsilon_{r,I}$ is obtained with the 340 °C sample. It is worth mentioning that the Ag specimen with RTA at 340 °C is again the best film

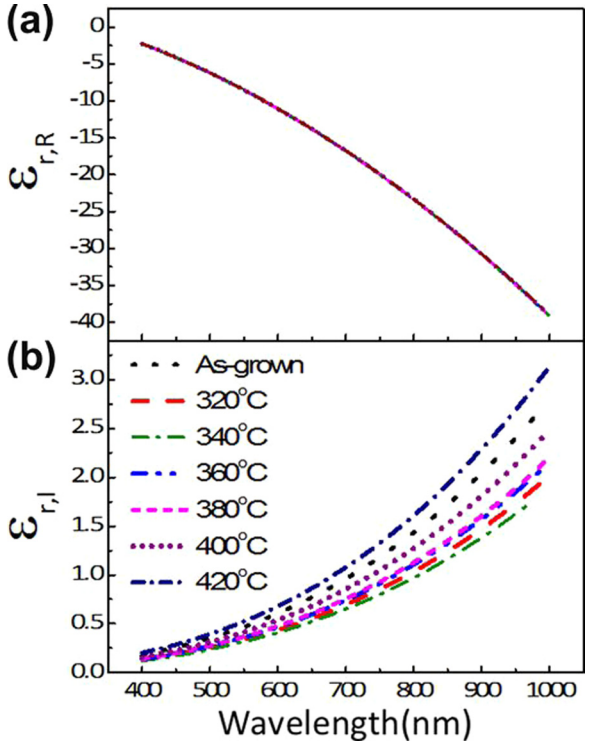

FIG. 7. (Color online) (a) Extracted real part ($\varepsilon_{r,R}$) and (b) imaginary part ($\varepsilon_{r,I}$) of complex relative dielectric constant of all samples.

and is comparable to the others.[15,27–29] Note that we have not considered the surface roughness effect on the extracted complex dielectric constants because it would not significantly affect the obtained values, particularly for the 340 °C-RTA sample whose surface is quite smooth. The surface roughness effect can be corrected, for example, by using the effective medium approximation[29] if necessary.

IV. CONCLUSIONS

We have successfully grown a low optical loss single-crystalline Ag thin film for the visible and near-infrared regime by using an easy and cost-effective method. The Ag thin film is deposited by e-gun evaporation on a carefully cleaned Si substrate followed by post rapid thermal annealing treatments with different temperatures in the flowing nitrogen atmosphere. By characterizing the crystal structure, surface morphology, and optical reflectivity spectra, an optimized condition for post thermal treatment has been obtained at 340 °C. The deposited Ag thin film shows excellent crystal quality with a clear FCC diffraction pattern, a sharp Ag single crystalline XRD diffraction peak with a FWHM value of 0.3°, and surface roughness RMS value of 0.46 nm. Moreover, low loss optical properties with high reflectivity and low damping characteristics are demonstrated in our Ag film, which shall be useful to develop plasmonics and nano-optoelectronic devices.

ACKNOWLEDGMENTS

The authors acknowledge the financial support from NSC and from ATU program of MOE in Taiwan. The equipment support from CNST and NFC at NCTU is appreciated.

[1]R. F. Oulton, V. J. Sorger, T. Zentgraf, R. M. Ma, C. Gladden, L. Dai, G. Bartal, and X. Zhang, Nature **461**, 629 (2009).
[2]M. J. H. Marell, B. Smalbrugge, E. J. Geluk, P. J. van Veldhoven, B. Barcones, B. Koopmans, R. Nötzel, M. K. Smit, and M. T. Hill, Opt. Express **19**, 15109 (2011).
[3]C.-Y. Wu, C.-T. Kuo, C.-Y. Wang, C.-L. He, M.-H. Lin, H. Ahn, and S. Gwo, Nano Lett. **11**, 4256 (2011).
[4]Y.-J. Lu *et al.*, Science **337**, 450 (2012).
[5]K. Ding, M. T. Hill, Z. C. Liu, L. J. Yin, P. J. van Veldhoven, and C. Z. Ning, Opt. Express **21**, 4728 (2013).
[6]C.-Y. Lu, S.-W. Chang, S. L. Chuang, T. D. Germann, U. W. Pohl, and D. Bimberg, Semicond. Sci. Technol. **26**, 014012 (2011).
[7]M. T. Hill *et al.*, Opt. Express **17**, 11107 (2009).
[8]M. T. Hill, J. Opt. Soc. Am. B **27**, B36 (2010).
[9]P. R. West, S. Ishii, G. V. Naik, N. K. Emani, V. M. Shalaev, and A. Boltasseva, Laser Photonics Rev. **4**, 795 (2010).
[10]S.-W. Lin, J.-Y. Wu, S.-D. Lin, M.-C. Lo, M.-H. Lin, and C.-T. Liang, Jpn. J. Appl. Phys. **52**, 045801 (2013).
[11]T. Hanawa and K. Oura, Jpn. J. Appl. Phys., Part 1 **16**, 519 (1977).
[12]M. H. Hoegen, T. Schmidt, M. Henzler, G. Meyer, D. Winau, and K. H. Rieder, Surf. Sci. **331**, 575 (1995).
[13]A. R. Smith, K. J. Chao, Q. Niu, and C. K. Shih, Science **273**, 226 (1996).
[14]W. Chen, M. D. Thoreson, S. Ishii, A. V. Kildishev, and V. M. Shalaev, Opt. Express **18**, 5124 (2010).
[15]J. H. Park, P. Ambwani, M. Manno, N. C. Lindquist, P. Nagpal, S.-H. Oh, C. Leighton, and D. J. Norris, Adv. Mater. **24**, 3988 (2012).
[16]N. Fang, H. Lee, C. Sun, and X. Zhang, Science **308**, 534 (2005).
[17]D. O. S. Melville and R. J. Blaikie, Opt. Express **13**, 2127 (2005).
[18]D. O. S. Melville, R. J. Blaikie, and C. R. Wolf, Appl. Phys. Lett. **84**, 4403 (2004).
[19]Y. Xiong, Z. Liu, C. Sun, and X. Zhang, Nano Lett. **7**, 3360 (2007).
[20]Z. Jacob, L. V. Alekseyev, and E. Narimanov, J. Opt. Soc. Am. A **24**, A52 (2007).
[21]X. Guo, M. Qiu, J. Bao, B. J. Wiley, Q. Yang, X. Zhang, Y. Ma, H. Yu, and L. Tong, Nano Lett. **9**, 4515 (2009).
[22]A. L. Pyayt, B. Wiley, Y. Xia, A. Chen, and L. Dalton, Nat. Nanotechnol. **3**, 660 (2008).
[23]M. A. Noginov, G. Zhu, M. Mayy, B. A. Ritzo, N. Noginova, and V. A. Podolskiy, Phys. Rev. Lett. **101**, 226806 (2008).
[24]M. Fox, *Optical Properties of Solids* (Oxford, New York, 2010), pp. 180–213.
[25]S. L. Chuang, *Physics of Photonic Devices* (Wiley, NJ, 2008), pp. 181–225.
[26]J. D. Jackson, *Classical Electrodynamics* (Wiley, NJ, 1998), pp. 237–294.
[27]P. B. Johnson and R. W. Christy, Phys. Rev. B **6**, 4370 (1972).
[28]E. D. Palik, *Handbook of Optical Constants of Solids I* (Elsevier, CA, 1997), pp. 353–355.
[29]J. H. Park, P. Nagpal, S.-H. Oh, and D. J. Norris, Appl. Phys. Lett. **100**, 081105 (2012).